

PAPER • OPEN ACCESS

# Floquet engineering of magnetism in topological insulator thin films

To cite this article: Xiaoyu Liu *et al* 2023 *Electron. Struct.* **5** 024002

View the [article online](#) for updates and enhancements.

## You may also like

- [A review of angle-resolved photoemission spectroscopy study on topological magnetic material family of  \$\text{MnBi}\_2\text{Te}\_4\$](#)   
Zhicheng Jiang, Jiayu Liu, Zhengtai Liu et al.
- [An efficient implementation of analytical nuclear gradients for linear-response time-dependent density functional theory in the plane wave basis](#)  
Jie Liu, Wei Hu and Jinlong Yang
- [Hard and soft materials: putting consistent van der Waals density functionals to work](#)  
Carl M Frostenson, Erik Jedvik Granhed, Vivekanand Shukla et al.



## PAPER

## OPEN ACCESS

## RECEIVED

27 November 2022

## REVISED

26 February 2023

## ACCEPTED FOR PUBLICATION

4 April 2023

## PUBLISHED

14 April 2023

Original Content from this work may be used under the terms of the [Creative Commons Attribution 4.0 licence](#).

Any further distribution of this work must maintain attribution to the author(s) and the title of the work, journal citation and DOI.



# Floquet engineering of magnetism in topological insulator thin films

Xiaoyu Liu<sup>1,2,9</sup>, Benshu Fan<sup>1</sup>, Hannes Hübener<sup>2</sup>, Umberto De Giovannini<sup>2,3</sup>, Wenhui Duan<sup>1,4,5</sup>, Angel Rubio<sup>2,6,7,\*</sup> and Peizhe Tang<sup>2,8,\*</sup>

<sup>1</sup> State Key Laboratory of Low-Dimensional Quantum Physics, Department of Physics, Tsinghua University, Beijing 100084, People's Republic of China

<sup>2</sup> Max Planck Institute for the Structure and Dynamics of Matter and Center for Free-Electron Laser Science, Luruper Chaussee 149, 22761 Hamburg, Germany

<sup>3</sup> Università degli Studi di Palermo, Dipartimento di Fisica e Chimica Emilio Segrè, via Archirafi 36, I-90123 Palermo, Italy

<sup>4</sup> Institute for Advanced Study, Tsinghua University, Beijing 100084, People's Republic of China

<sup>5</sup> Collaborative Innovation Center of Quantum Matter, Beijing 100084, People's Republic of China

<sup>6</sup> Nano-Bio Spectroscopy Group, Departamento de Física de Materiales, Universidad del País Vasco UPV/EHU- 20018 San Sebastián, Spain

<sup>7</sup> Center for Computational Quantum Physics, Flatiron Institute, 162 Fifth Avenue, New York, NY 10010, United States of America

<sup>8</sup> School of Materials Science and Engineering, Beihang University, Beijing 100191, People's Republic of China

<sup>9</sup> Current address: Department of Materials Science and Engineering, University of Washington, Seattle, WA, United States of America.

\* Authors to whom any correspondence should be addressed.

E-mail: [angel.rubio@mpsd.mpg.de](mailto:angel.rubio@mpsd.mpg.de) and [peizhet@buaa.edu.cn](mailto:peizhet@buaa.edu.cn)

**Keywords:** Floquet theory, quantum quenching, magnetically doped topological insulator thin film

## Abstract

Dynamic manipulation of magnetism in topological materials is demonstrated here via a Floquet engineering approach using circularly polarized light. Increasing the strength of the laser field, besides the expected topological phase transition (PT), the magnetically doped topological insulator thin film also undergoes a magnetic PT from ferromagnetism to paramagnetism, whose critical behavior strongly depends on the quantum quenching. In sharp contrast to the equilibrium case, the non-equilibrium Curie temperatures vary for different time scale and experimental setup, not all relying on change of topology. Our discoveries deepen the understanding of the relationship between topology and magnetism in the non-equilibrium regime and extend optoelectronic device applications to topological materials.

## 1. Introduction

The interplay between magnetism and topological state has attracted considerable attention in recent studies. Many exotic topological particles and macroscopic quantum phenomena have been realized, including Weyl fermions [1–7], antiferromagnetic Dirac fermions [8, 9], quantum anomalous Hall (QAH) effect [10–16], antiferromagnetic topological insulators (TI) [17, 18], and axion insulators [18–23]. In real materials, the emergence of magnetism breaks the time reversal symmetry and the exchange coupling can drive the system into a new topological phase. For example, the long-range ferromagnetic (FM) order can be formed by doping TI films with magnetic ions [10, 24–27], the Zeeman coupling splits degenerate bands and drives TI thin film to be a Chern insulator with the quantized edge conductance [11–15]. Meanwhile, in turn, these topological bands, both in bulk and on the surface, have the ability to form or enhance long-range ferromagnetism [10, 24, 25, 27]. Therefore, from a practical point of view, finding an efficient way to manipulate magnetic and topological orders will trigger intense research in the fields of spintronics and quantum information processing. The electric field-controlled ferromagnetism has been proposed theoretically [28] and achieved experimentally in a magnetically doped TI (MDTI) thin film [29], which is possible to be used in spintronic devices [28].

Different from conventional manipulations of topology and magnetism in equilibrium, Floquet engineering via ultrafast optical driving provides a new possibility to tune electronic properties of host

material dynamically in non-equilibrium [30–35]. The strong interaction of photons with charges, spins, and angular momenta can drive the system to a steady Floquet state, dramatically changing Floquet band structure and charge population [30, 32, 33]. This approach provides a new degree of freedom to manipulate the magnetic order [36, 37] and novel topological states [30, 31, 38–44]. By using Floquet engineering, semiconductor quantum wells [45–47] and two-dimensional (2D) materials [41, 48] can be driven to behave as Floquet TIs. Light-induced Hall conductance is predicted and observed in graphene, pointing towards a topological origin [49–56].

Herein, in the framework of the Floquet theorem, we study the electronic and magnetic properties of periodically driven TI and MDTI thin films. Under circularly polarized light (CPL), Floquet bands of steady states can be well-tuned, resulting in a photon-induced topological phase transition (PT). Furthermore, we develop a Floquet linear-response theory to calculate the magnetic susceptibility in MDTI thin films. We find that CPL can reduce its magnetic susceptibility, driving FM thin films to be paramagnetic. The decreasing behavior of the magnetic PT strongly depends on quantum quenching and dissipation. For example, in contrast to that on long time scale, the magnetic susceptibility decreases more quickly in a short time scale with the change of the laser field, resulting in a lower Curie temperature ( $T_C$ ) correspondingly. Our work provides a new way to manipulate topological and magnetic properties in MDTI thin films via an optical approach and our predictions can be measured by magneto-optic and transport experiments.

## 2. Method

Under CPL, a non-equilibrium Floquet state is possible to be formed in quantum materials [31, 39, 40, 54]. In the Floquet theory [57–59], we can solve the time-dependent Schrödinger equation in the Hilbert space  $\mathcal{H}$  via mapping it to a time-independent infinite eigenvalue problem in an extended Hilbert space  $\mathcal{H} \otimes \mathcal{L}_T$  [60, 61], where  $\mathcal{L}_T$  represents the space of ‘multi-photon-dressed’ states. Finally, the resulting states are the Floquet bands, whose occupations strongly depend on the quantum quenching and dissipation details.

The band structure and charge distribution in the initial equilibrium are shown in figure 1(a). If we switch on the laser suddenly and measure the physical observable in a short time (such as magneto-optical Kerr rotation angle [62], schematically shown in figure 1(d)), the time scale for this system to reach a steady state is short compared to the period of the laser [50, 51]. In this way (see figure 1(b)), electrons tend to stay in their original bands, and the population of the quenched Floquet system is mainly determined by the overlapping matrix between final and original states [61]. This approach is named the Sudden Approximation [50, 51]. On the other limit (see figure 1(c)), if the measurement is performed over a long time (such as anomalous Hall effect in ultrafast transport [55, 56], schematically shown in figure 1(e)), excited electrons are relaxed and the population of the Floquet state behaves like a Floquet Fermi–Dirac distribution with effective chemical potentials for electrons and holes [47, 63]. In this work, we calculate magnetic properties, especially the magnetic susceptibilities for MDTI thin films in these two extreme situations by the Floquet linear response theory [49, 51, 61, 64, 65].

## 3. Results

### 3.1. Effective model

To study MDTI thin films under CPL, we start from the 2D effective Hamiltonian for TI thin films [10, 28, 66, 67],

$$H_0(\mathbf{k}) = \epsilon(\mathbf{k}) + v_F k_y \sigma_1 \otimes \tau_3 - v_F k_x \sigma_2 \otimes \tau_3 + m(\mathbf{k}) \cdot \mathbf{I} \otimes \tau_1 \quad (1)$$

written in the basis of  $\{|u \uparrow\rangle, |u \downarrow\rangle, |d \uparrow\rangle, |d \downarrow\rangle\}$ ,  $\uparrow$  and  $\downarrow$  stand for the spin degree of freedom,  $|u\rangle$  and  $|d\rangle$  are surface states on the upper and down surfaces of the TI thin film.  $\sigma_i$  and  $\tau_i$  ( $i = 1, 2, 3$ ) are the Pauli matrices for spin and orbital,  $k_{x,y}$  is the momentum in reciprocal space,  $v_F$  is the Fermi velocity,  $\epsilon(\mathbf{k}) = \epsilon_0 + \epsilon_2(k_x^2 + k_y^2)$  is the energy shift, and  $m(\mathbf{k}) = m_0 + m_2(k_x^2 + k_y^2)$  is the coupling between  $|u\rangle$  and  $|d\rangle$ . Due to the inter-surface coupling, a finite gap opens around the  $\Gamma$  point and topological properties of thin films are determined by the sign of  $m_0 m_2$  [10, 61, 68].

We include the effect of CPL by the Peierls substitution  $\mathbf{k} \rightarrow \mathbf{k} - e\mathbf{A}(t)$ , where  $\mathbf{A}(t)$  is the laser amplitude and  $e$  is the electron charge.  $\mathbf{A}(t) = A(\cos \omega t, \sin \omega t, 0)$  is for right-hand CPL,  $\omega$  is the frequency with the photon energy of 3 eV. Time-independent infinite Floquet Hamiltonian  $H_F(\mathbf{k})$  can be obtained in the framework of the Floquet theory [61]. By diagonalizing  $H_F(\mathbf{k})$  with a cut-off on the frequency domain, we obtain the Floquet band structures [61]. In the high-frequency limit ( $\hbar\omega \gg W$ ,  $\hbar$  is the reduced Planck constant and  $W$  is the bandwidth of the thin film), the low order expansion [30, 31, 60, 69] can be employed to reduce the infinite  $H_F(\mathbf{k})$  to an effective Hamiltonian  $H_{\text{eff}}(\mathbf{k})$  with the form of:

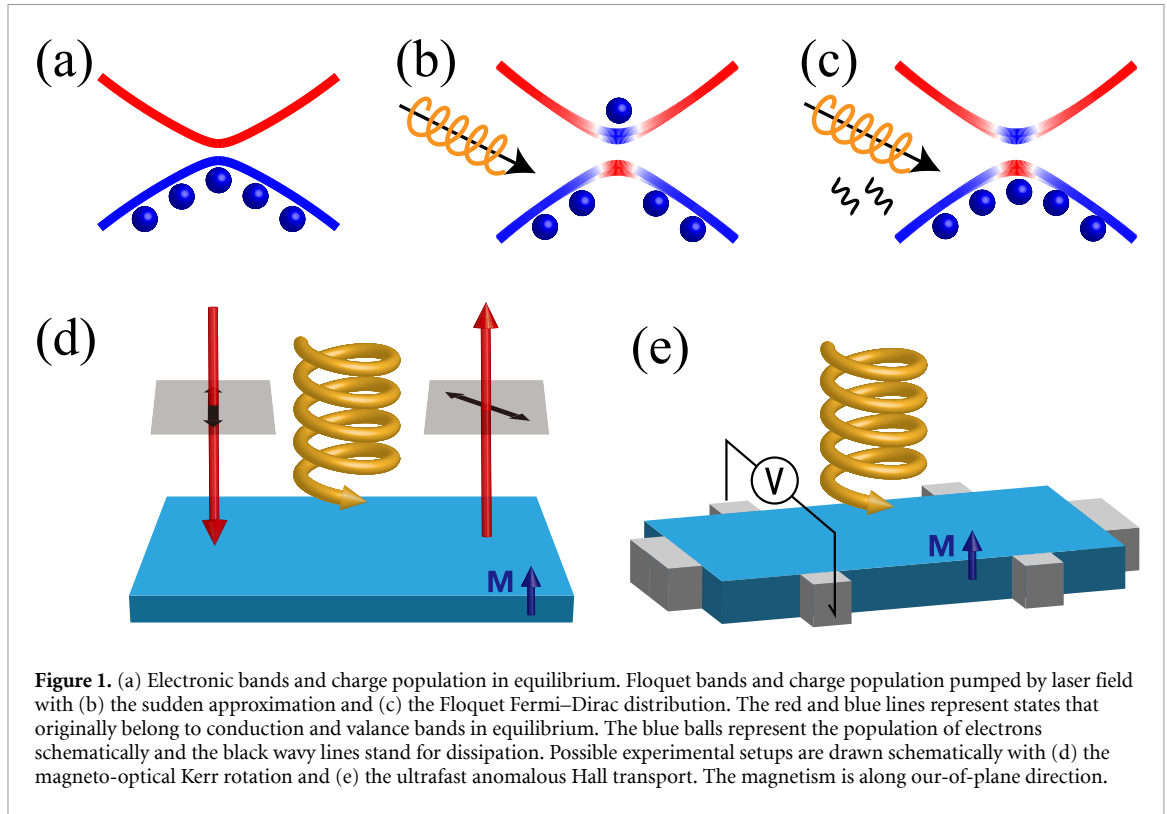


**Figure 1.** (a) Electronic bands and charge population in equilibrium. Floquet bands and charge population pumped by laser field with (b) the sudden approximation and (c) the Floquet Fermi–Dirac distribution. The red and blue lines represent states that originally belong to conduction and valance bands in equilibrium. The blue balls represent the population of electrons schematically and the black wavy lines stand for dissipation. Possible experimental setups are drawn schematically with (d) the magneto-optical Kerr rotation and (e) the ultrafast anomalous Hall transport. The magnetism is along our-of-plane direction.

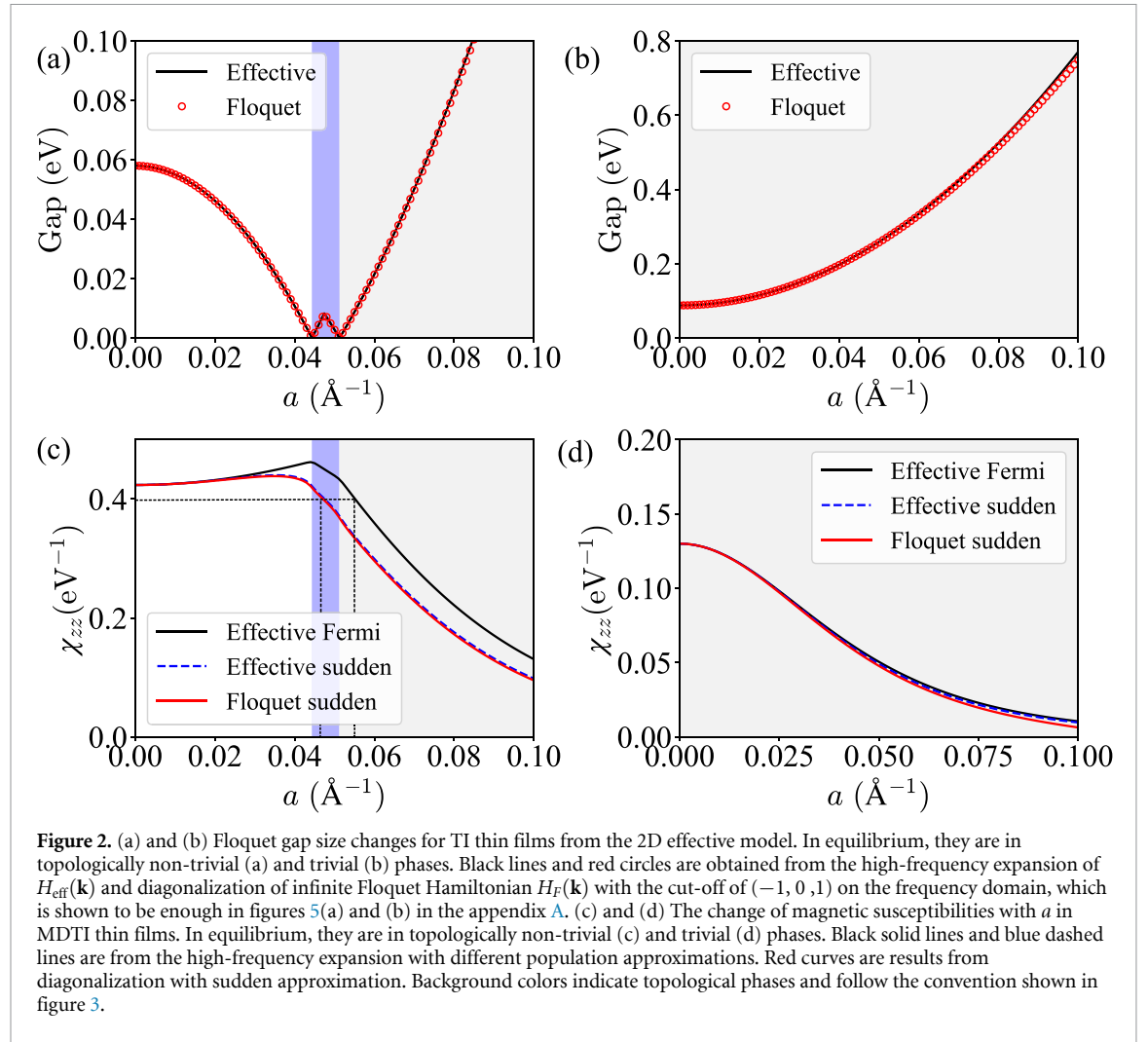
$$H_{\text{eff}}(\mathbf{k}) = H_0(\mathbf{k}) + \epsilon_2 a^2 + m_2 a^2 \cdot \mathbf{I} \otimes \tau_1 + \frac{a^2}{\hbar\omega} v_F^2 \cdot \sigma_3 \otimes \tau_0 - 2 \frac{a^2}{\hbar\omega} v_F m_2 (k_x \sigma_1 + k_y \sigma_2) \otimes \tau_2. \quad (2)$$

Here  $a = eA$  is the effective laser amplitude with unit  $\text{\AA}^{-1}$ . This Hamiltonian has the same dimension as the original  $H_0(\mathbf{k})$ . Its second term corrects  $\epsilon_0$  (see equation (1)) and results in the total energy shift. The third term modifies  $m_0 \rightarrow m_0 + m_2 a^2$  and induces a topological PT when the laser amplitude is large enough. The light intensity that triggers the topological PT in our system is around  $10^9$ – $10^{11} \text{ W cm}^{-2}$ , which is experimentally feasible [43, 70, 71]. Interestingly, these terms do not depend on the laser frequency but rely on laser amplitude only. Moreover, CPL introduces two new terms at the end of equation (2), which are proportional to  $a^2/\hbar\omega$  and smaller compared to correction terms under the high-frequency limit. The first one is momentum-independent and acts like the exchange coupling due to time reversal symmetry breaking. The second one is momentum-dependent and has a negligible effect for electronic bands around  $\Gamma$  point. To sum up, the change of band structures for TI thin films under CPL is dominated by correction terms and slightly modified by the frequency-dependent terms.

Numerical results demonstrate the analysis above is correct. In figures 2(a) and (b), we show the calculated direct Floquet gap size for TI thin films from the 2D effective model when fixing the frequency and changing the amplitude of the driving laser. In equilibrium, we use parameters shown in [28] for  $H_0(\mathbf{k})$  where 4 quintuple layer (QL) TI thin film is in the quantum spin Hall (QSH) phase ( $m_0 m_2 < 0$ ) and 3QL thin film is a normal insulator ( $m_0 m_2 > 0$ ). When the laser is turned on, their electronic band structures are modified. Two curves with different colors illustrate the gap size in the Floquet band structures obtained through the high-frequency expansion (black line) and direct diagonalization respectively (red circles). The good agreement between the two methods suggests that current parameter settings reach the high-frequency limit.

When we increase the laser amplitude  $a$  for 4QL thin film, its Floquet gap at the  $\Gamma$  point decreases at first, undergoes two gap-closing processes, and finally increases again (see figure 2(a)). Such evolution indicates topological PTs from a NIB phase to a QAH phase, and finally to a NIA phase. Here, NIB is a state with a Floquet band structure similar to the QSH insulator without topological protection [28]. NIA stands for a normal insulator. The QAH phase (blue region) mainly originates from the light-induced exchange coupling in TI film. Since the exchange term is proportional to  $a^2/\hbar\omega$ , its phase region is very narrow in the high frequency. In contrast to the 4QL thin film, we observe no gap-closing process as the increase of light amplitude for 3QL film, meaning that it persists in NIA phase (see figure 2(b)).

When TI thin films are doped with magnetic ions, such as Cr [11, 26] and V [15] atoms, the long-range FM order can be formed in equilibrium. If we keep MDTI thin films insulating, the ferromagnetism is



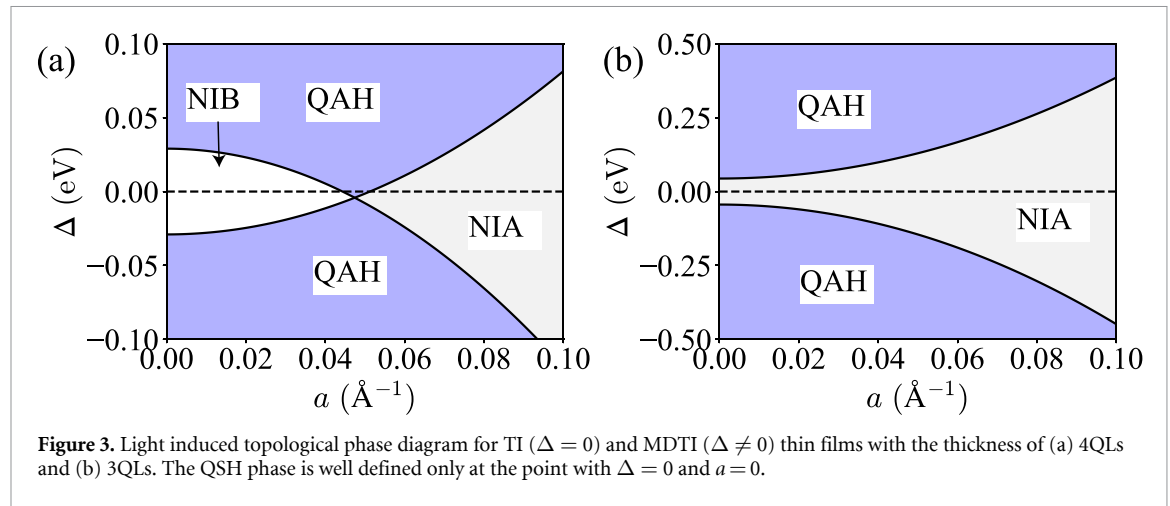
induced by the van Vleck mechanism [10, 26, 27, 61]. The low energy electronic structure around the  $\Gamma$  point can be described by the Hamiltonian:  $H_0^{\text{FM}}(\mathbf{k}) = H_0(\mathbf{k}) + \Delta \cdot \sigma_3 \otimes I$ , where  $\Delta$  is the Zeeman term arising from FM order and is determined by the density of dopants and the magnetic susceptibility [10]. Interestingly, MDTI thin films undergo a FM to paramagnetic transition via changing dopant densities, accompanied by a topological PT [27]. Currently, the experimental preparation [11–13] and manipulation techniques [29] of MDTI thin films are relatively mature, and ultrafast laser pulse can be used to drive them far from equilibrium [39, 40].

We can fix the density of dopants in MDTI thin films to guarantee their equilibrium states to be FM for 4QLs and paramagnetic for 3QLs, and then apply CPL to drive the systems to the Floquet states. Thus the change of magnetic properties induced by the laser field is determined by the magnetic susceptibilities of electrons  $\chi_{zz}^{\text{Floq}}$ , and it is calculated for Floquet states by the Kubo linear-response theory [61]:

$$\chi_{zz}^{\text{Floq}} = \sum_{\alpha \in \text{FBZ}, \beta, k} 2f_{\alpha} \frac{|\langle \phi_{\alpha}(t) | s_z | \phi_{\beta}(t) \rangle|^2}{\epsilon_{\beta} - \epsilon_{\alpha}} \quad (3)$$

where  $\alpha$  and  $\beta$  label the Floquet states,  $\phi_{\alpha}(t)$  is the Floquet wavefunction with quasienergy  $\epsilon_{\alpha}$ ,  $f_{\alpha}$  is its population,  $s_z$  is the spin operator along  $z$  direction, and Floquet Brillouin zone (FBZ) [61]. In non-equilibrium, the occupation of Floquet states strongly depends on the frequency and amplitude of the driving laser [56, 72] as well as dissipation to a bath [47]. Here we only consider steady Floquet states formed in two limited situations with high frequency.

As shown in figures 2(c) and (d), the magnetic PT points change with different quenching schemes when the light intensity increases, although the trend of their variation  $\chi_{zz}^{\text{Floq}}$  behaves similarly. For the 4QL MDTI thin film, the magnetic susceptibility increases slowly in the NIB phase and drops quickly in the QAH and NIA phases. When  $\chi_{zz}^{\text{Floq}}$  reaches the critical value resulting in a magnetic PT, we observe different critical points  $a_c^{\text{FM}}$  for different quenching schemes (marked by a black dashed line in figure 2(c)). Compared with



$T_C$  in equilibrium, CPL decreases its value by the Floquet engineering. Such decreasing tendency is mainly contributed by the change of gap size and matrix elements shown in equation (3).

In the regime of the sudden approximation, the critical value  $a_c^{\text{FM}}$  is smaller than that in the Floquet Fermi–Dirac distribution. Furthermore,  $a_c^{\text{FM}}$  in the two kinds of quenched schemes do not have the same value as the critical amplitude  $a_c^T$  for topological PT. Therefore, we conclude that, besides the modulation of energy levels, the light also changes the population of Floquet states, which plays an essential role in determining the magnetic behavior. This population dependence is unique for non-equilibrium states in contrast to previous studies [27, 28]. For 3QLs (see figure 2(d)), the decreasing behavior of  $\chi_{zz}^{\text{Floc}}$  is observed but the entire system remains in the paramagnetic phase.

The topological phase diagram is shown in figure 3 for MDTI thin films, whose results are from the effective model considering the FM exchange coupling and the influence of CPL. If the intrinsic system is initially in QSH state (e.g. 4QLs), there are three phase regions as shown in figure 3(a), including a QAH phase and two trivial insulating phases NIA and NIB. The asymmetric feature with respect to  $\Delta$  is due to the additional exchange terms induced by the driving laser (see equation (2)). For an initial state without topology (e.g. 3QLs), the phase diagram is much simpler with only transitions from the normal insulator to QAH state when  $\Delta$  is large enough. We need to point out that under the aforementioned laser intensity, the system is possible to generate a static magnetic moment due to the nonlinear Edelstein effect [73]. However, it only shifts the critical points of the PT, rather than changing the qualitative conclusions.

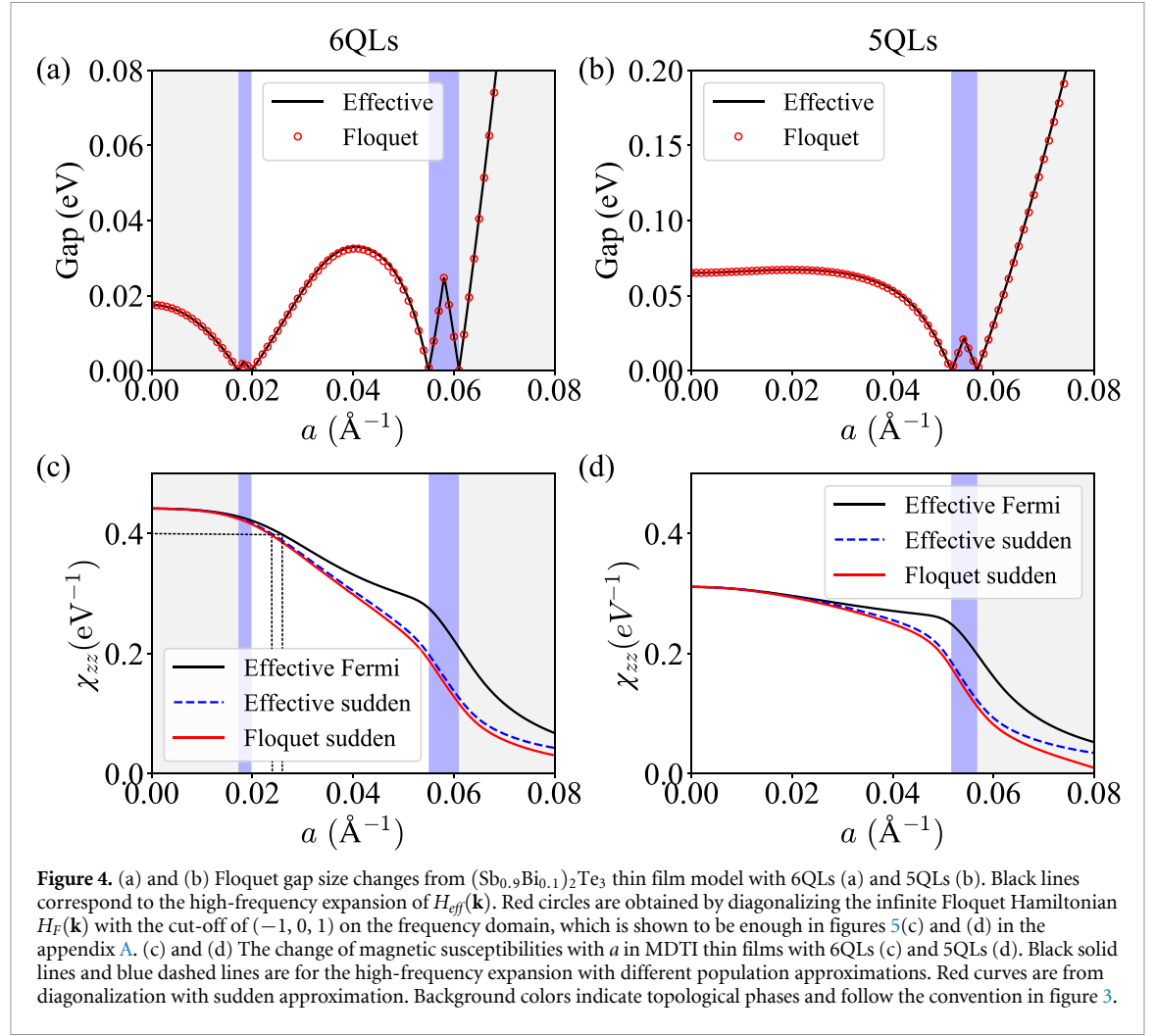
### 3.2. Thin film model

The above discussions are based on the effective Hamiltonian. It is a relatively simple model to give us a clear physical picture of light-induced magnetic and topological PTs, but cannot predict all details precisely without including the contributions from quantum well states. To confirm the validity of the picture and describe a more realistic situation in experiments, we choose  $(\text{Sb}_{0.9}\text{Bi}_{0.1})_2\text{Te}_3$  as an example, which has been fabricated in previous experiments [29, 66]. We consider its three-dimensional bulk Hamiltonian in a thin film construction with thickness  $d$  [61]. The confinement in the  $z$  direction quantizes the momentum on this axis. The contribution from QWSs can be fully considered in the thin film model [28, 68, 74, 75]. In our equilibrium calculations,  $(\text{Sb}_{0.9}\text{Bi}_{0.1})_2\text{Te}_3$  thin film of 6QL is topologically trivial and its 5QL thin film is a QSH insulator.

To understand the effect induced by CPL in the thin film model, we do similar calculations as those by using the effective Hamiltonian. Figure 4 shows direct Floquet gap sizes and magnetic susceptibilities for  $(\text{Sb}_{0.9}\text{Bi}_{0.1})_2\text{Te}_3$  thin films under CPL. Similar to results from the simple model, light-induced topological and magnetic PTs exist in intrinsic and doped thin films. A more complicated topological phase diagram is observed for 6QLs when  $a$  increases. They go through phases from NIA to QAH, to NIB, to QAH again, and finally enter a NIA phase. Such oscillatory crossover behaviour is dominated by quantum well states [61] and cannot be captured by the simple 2D effective model. For the 5QL thin film, the topological PT driven by the light is similar to that shown in figure 2(a), suggesting its topological characters can be well described by the 2D effective Hamiltonian.

When magnetic ions are doped at the density used in figure 2, the MDTI thin film of 6QL becomes FM while 5QLs do not, indicating that the 2D effective model is not well suited to describe the realistic magnetic properties for the 5QL thin film. The magnetic susceptibilities of the Floquet states decrease with the increase of light intensity and the slopes change differently in different topological phases.  $a_c^{\text{FM}}$  in magnetic PTs also





depends on the quantum quenching and does not correspond directly to the critical value of the topological PT. These results obtained from realistic thin film models are consistent with the conclusions from the 2D effective model, confirming the validity of our physical picture.

#### 4. Conclusion

Using the Floquet theory, we study topological and magnetic properties for TI and MDTI thin films under CPL. In the high-frequency limit, topological PTs can be induced in TI thin films by increasing the intensity of the driving laser. Applying the same setup to MDTI thin films, we find magnetic PTs from FM to paramagnetic phases and their critical behaviors depend on the quantum quenches that influence the non-equilibrium charge population. Based on previous discussions using the Floquet-Green's function method [72], we argue that the high-frequency approximation is reasonable in a considerably large frequency regime, even when  $\hbar\omega$  is comparable to  $W$ . On the other hand, when  $\hbar\omega$  is smaller than  $W$  with the resonant photon absorption,  $\chi_{zz}^{\text{Floq}}$  still behaves similarly to the non-resonant case except in photon absorption regions [61]. Thus, we are convinced that our conclusion could apply in a large parameter regime.

The phenomena proposed in this work are possible to be observed by different experimental setups. In pump-probe detection of the polar Kerr-rotation angle [62], the population effect could be described by the sudden approximation and the change of magnetism could be measured. Meanwhile, the Floquet Fermi-Dirac distribution is a good approximation for the transport measurement, such as the ultrafast anomalous Hall effect by laser-triggered photoconductive switches [55, 56]. In fact, due to the high photon energy and electric field strength required in our system, resonant interband absorption may occur and damage the sample during the experiment. However, some studies have shown that Floquet states can survive despite resonant absorption [43, 71]. We expect that light-driven topological and magnetic PTs can be realized in TI and MDTI thin films.

## Data availability statement

All data that support the findings of this study are included within the article (and any supplementary files).

## Acknowledgment

X L, B F and W D acknowledge financial supports from the Ministry of Science and Technology of China (Grant No. 2016YFA0301001), the National Natural Science Foundation of China (Grant No. 51788104), and the Beijing Advanced Innovation Center for Future Chip (ICFC). A R, H H, and U D G acknowledge financial supports from the European Research Council (ERC-2015-AdG-694097). The Flatiron Institute is a division of the Simons Foundation. P T was supported by the National Natural Science Foundation of China (Grants No. 12234011) and the Open Research Fund Program of the State Key Laboratory of Low-Dimensional Quantum Physics.

## Appendix A. Floquet theory

When a system is driven by the laser field, it is possible to enter a steady state with discrete time translation symmetry, named the Floquet state. Its Hamiltonian is a time-periodic  $H(t) = H(t + T)$  with period  $T = 2\pi/\omega$ , where  $\omega$  is the frequency of the light. For such kind of system, according to the Floquet theory, the solutions of Schrödinger equation have the form  $\psi_\alpha(t) = e^{-i\epsilon_\alpha t}\phi_\alpha(t)$ , in which  $e^{-i\epsilon_\alpha t}$  is an aperiodic phase factor and  $\phi_\alpha(t) = \phi_\alpha(t + T)$  is a periodic function. The Floquet states  $\psi_\alpha(t)$  are eigenstates of the evolution operator over one period  $U(t + T, t)$  [60],  $\epsilon_\alpha$  is the Floquet quasi-energy, and  $\phi_\alpha(t)$  is the Floquet mode.

Periodic Floquet mode  $\phi_\alpha(t)$  can be expanded by discrete Fourier series  $\phi_\alpha(t) = \sum_m e^{-im\omega t} u_{\alpha,m}^m$ ,  $m \in \mathbb{Z}$ . When we substitute  $\psi_\alpha(t)$  into the Schrödinger equation and expand the Floquet modes, we obtain [49]:

$$\sum_n H_{mn}(\mathbf{k}) u_\alpha^n(\mathbf{k}) = [\epsilon_\alpha(\mathbf{k}) + m\hbar\omega] u_\alpha^m(\mathbf{k}) \quad (\text{A1})$$

where  $H_{mn}(\mathbf{k}) = \frac{1}{T} \int_0^T dt H(\mathbf{k}, t) e^{i(m-n)\omega t}$  and is time-independent. The infinite matrix  $(H_{mn} - \delta_{mn}m\hbar\omega)$  is denoted as the infinite Floquet Hamiltonian  $H_F(\mathbf{k})$  [49]. This time-independent equation is defined in the extended Hilbert space  $\mathcal{H} \otimes \mathcal{L}_T$ , in which  $\mathcal{H}$  is the original Hilbert space for the intrinsic system and  $\mathcal{L}_T$  is the space of  $T$ -periodic functions. In this work, the cut-off of the Floquet index  $m$  and  $n$  in the infinite Floquet Hamiltonian  $H_F(\mathbf{k})$  is chosen to be  $(-1, 0, 1)$ , which is shown to be sufficient in figure 5.

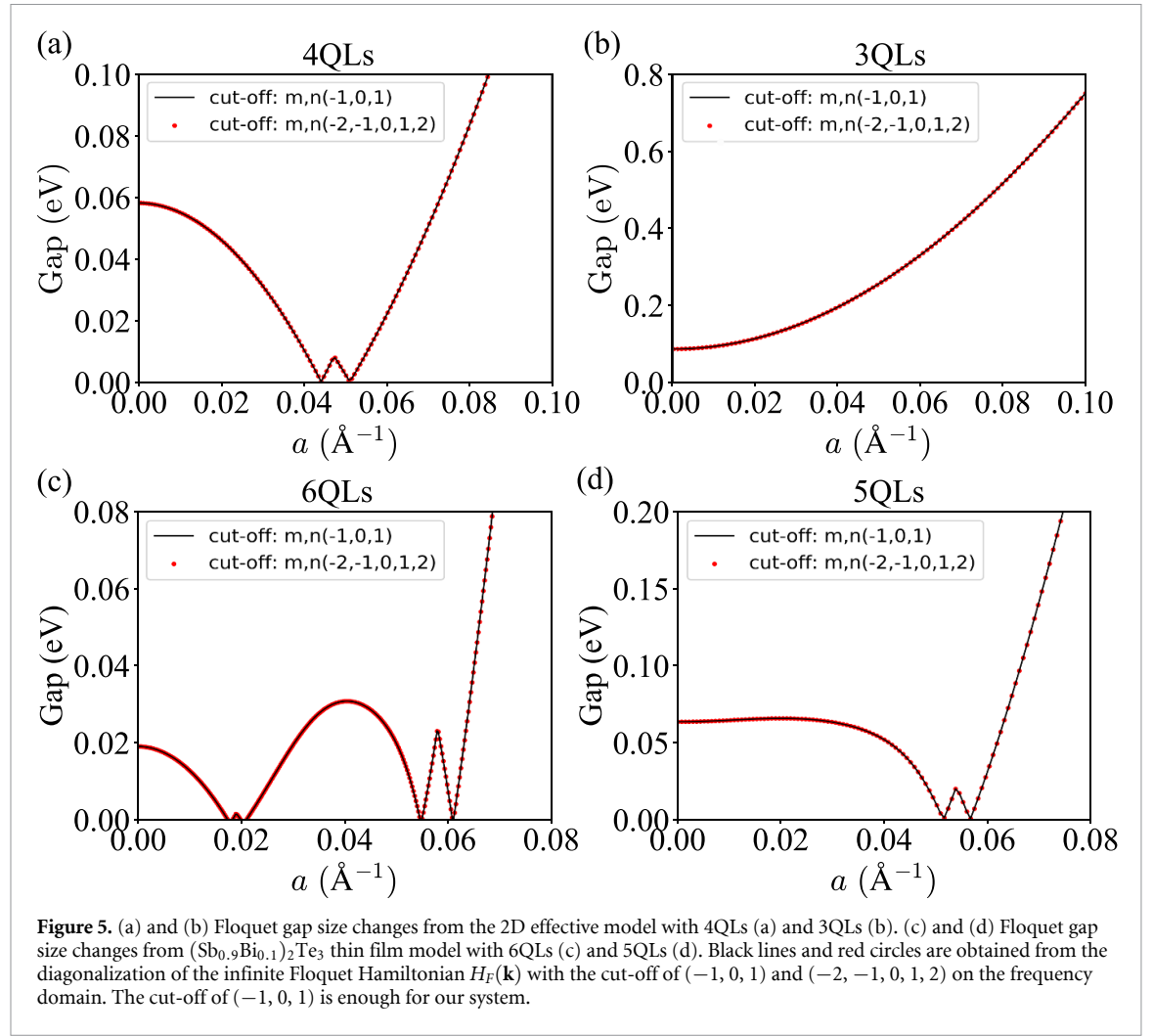
The number of independent Floquet states should coincide with the dimension of  $H(t)$ . This means the infinite eigenstates of  $H_F(\mathbf{k})$  are highly redundant. In fact, eigenstates whose eigenvalues differ by integer multiples of  $\hbar\omega$  are related. For example, the Floquet modes  $\phi_\alpha(t)$  and  $e^{im\omega t}\phi_\alpha(t)$  with eigenenergy  $\epsilon_\alpha$  and  $\epsilon_\alpha + m\hbar\omega$  represent the same Floquet state  $\psi_\alpha$ . To remove such redundancy, we focus on states with quasienergies lying inside one  $\hbar\omega$  region. Similar to the concept of the Brillouin zone (BZ), we name  $[-\frac{\hbar\omega}{2}, \frac{\hbar\omega}{2})$  as the first FBZ. As an example, FBZ is shown by the yellow background in figure 10.

Under the high-frequency limit, the diagonal blocks are dominated by  $m\hbar\omega$  term and weakly coupled with other blocks by  $H_{mn}(\mathbf{k})$ . By performing perturbation theory, the effective Hamiltonian [30, 31, 60, 69] can be derived as:

$$H_{\text{eff}}(\mathbf{k}) = H_{00} + \frac{[H_{10}, H_{01}]}{\hbar\omega} + O((\hbar\omega)^2). \quad (\text{A2})$$

Via applying this approach to the 2D effective thin film Hamiltonian (equation (1) in the main text), we get the time-independent Floquet effective Hamiltonian equation (2) in the main text.





## Appendix B. 2D effective model

In the main text, we show in figure 2(a) that for 4QL film there are two gap-closing points with the increase of the effective light amplitude  $a$ , indicating topological PTs. For clarity, we plot here the corresponding band structures for typical amplitudes, see figure 6.

The gap-closing points can be analytically obtained from the low-order expanded Floquet effective Hamiltonian  $H_{\text{eff}}(\mathbf{k})$  (see equation (2) in the main text). The eigenvalues of  $H_{\text{eff}}(\mathbf{k})$  are:

$$E_1 = \pm \sqrt{v_F^2 \left( \frac{2a^2}{\hbar\omega} m_2 + 1 \right)^2 k^2 + \left[ a^2 \left( \frac{v_F^2}{\hbar\omega} - m_2 \right) - m(k) \right]^2}$$

$$E_2 = \pm \sqrt{v_F^2 \left( \frac{2a^2}{\hbar\omega} m_2 - 1 \right)^2 k^2 + \left[ a^2 \left( \frac{v_F^2}{\hbar\omega} + m_2 \right) + m(k) \right]^2}. \quad (\text{B1})$$

Here  $m(k) = m_0 + m_2(k_x^2 + k_y^2)$ . Because the model system has particle-hole symmetry, the gap-closing points must occur at zero energy ( $E_1 = 0$  or  $E_2 = 0$ ). In total, there are two circumstances to host such condition with zero energy solutions.

Firstly, they can lie at  $k = 0$  with  $m_0 = -a^2(m_2 \pm \frac{v_F^2}{\hbar\omega})$ . Usually,  $\frac{v_F^2}{\hbar\omega}$  has small value compared to that of  $m_2$  [28] and can be ignored. Thus, the sign of  $m_0 m_2$  must be negative, meaning the system is in the QSH phase initially. The two critical amplitudes  $a$  for two topological transitions are separated by  $\Delta a \approx \frac{|m_0|^{1/2}}{|m_2|^{3/2}} \frac{v_F^2}{\hbar\omega}$  in the high-frequency limit. Such value is very small, corresponding to a narrow region for the QAH phase shown in figures 2(a) and (b) in the main text.

The other circumstance is at  $k \neq 0$  together with  $\frac{2a^2}{\hbar\omega} m_2 = 1$  and  $a^2(\frac{v_F^2}{\hbar\omega} + m_2) + m_0 = 0$ . Substituting the former condition into the latter one, we have  $\frac{\hbar\omega}{2} + \frac{v_F^2}{2m_2} + m_0 = 0$ . In the high-frequency limit,  $\hbar\omega \gg W \sim m_0$ , so we can not find a suitable solution for this condition.

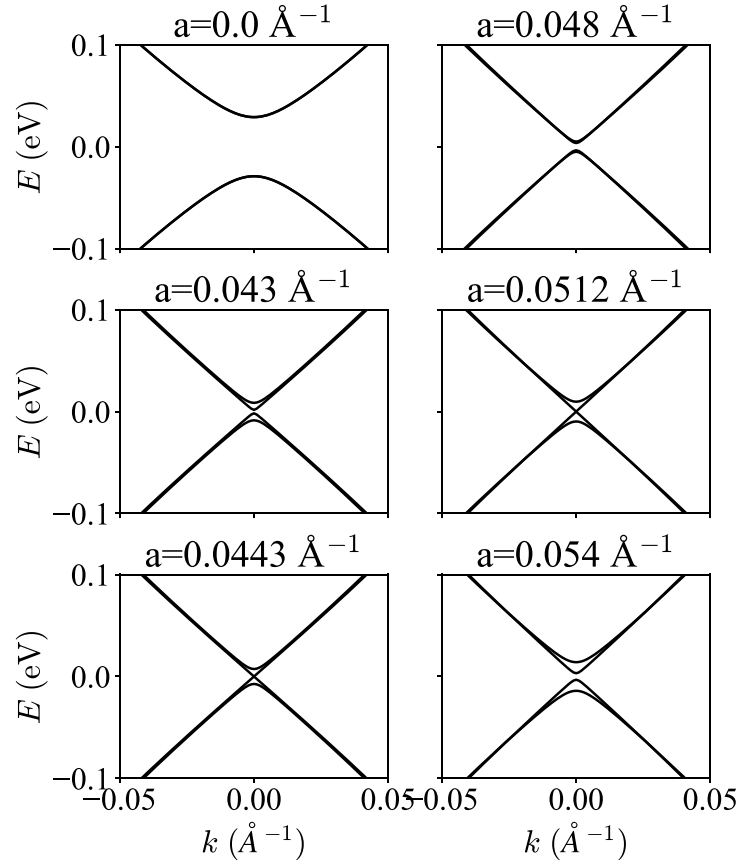


**Figure 6.** Band structures of  $H_{\text{eff}}(\mathbf{k})$  (equation (A2)) for the 2D effective model of 4QL at different light intensities.

### Appendix C. Kubo formula

We use the time-dependent Kubo formula derived from linear response theory to calculate the magnetic susceptibilities  $\chi_{zz}$  of the Floquet system. Following the notion in [64], we have:

$$\chi_{zz}(t, t') = -i\theta(t - t') \langle \Psi_0 | [s_z^I(t), s_z^I(t')] | \Psi_0 \rangle. \quad (\text{C1})$$

Here  $\Psi_0$  represents the initial state, the subscript  $I$  represents interaction picture,  $s_z$  is the spin operator along the  $z$  direction, and  $\theta(t, t')$  is the Heaviside function. Written in the Schrödinger picture, equation (C1) becomes,

$$\chi_{zz}(t, t') = -i\theta(t - t') \langle \Psi_0 | U(t_0, t) s_z U(t, t') s_z U(t', t_0) - U(t_0, t') s_z U(t', t) s_z U(t, t_0) | \Psi_0 \rangle \quad (\text{C2})$$

with the evolution operator [60]:

$$\begin{aligned} U(t, t') &= \sum_{\alpha \in \text{FBZ}} |\psi_\alpha(t)\rangle \langle \psi_\alpha(t')| \\ &= \sum_{\alpha \in \text{FBZ}} e^{-i\epsilon_\alpha(t-t')} |\phi_\alpha(t)\rangle \langle \phi_\alpha(t')| \end{aligned} \quad (\text{C3})$$

given by the Floquet state. If the system without laser driving is in thermal equilibrium, the initial state  $\Psi_0$  is a thermal ensemble. The response formula becomes,

$$\chi_{zz}(t, t') = -i\theta(t - t') \sum_i f_i \langle \psi_i | [s_z^I(t), s_z^I(t')] | \psi_i \rangle \quad (\text{C4})$$

where  $\psi_i$  represents the eigenstate of the initial equilibrium Hamiltonian and follows Fermi–Dirac distribution  $f_i$ .  $\chi_{zz}(t, t')$  depends on both  $t$  and  $t'$  in the Floquet systems due to the lack of time translation invariance. However, in reality, we only care about the mean response over several periods. This can be done by averaging over the mean time  $\frac{t+t'}{2}$  [51]. The static spin susceptibility is obtained by a further integration over  $t - t'$ .

## Appendix D. Sudden approximation

In this section, we show how we apply the sudden approximation to both  $H_{\text{eff}}(\mathbf{k})$  and  $H_F(\mathbf{k})$  in our calculations. We assume that the system is initially in thermal equilibrium, and for simplicity, we omit  $k$  summation in the following equations.

For Floquet effective Hamiltonian  $H_{\text{eff}}(\mathbf{k})$  in the Hilbert space of  $\mathcal{H}$ , after the light is turned on, the evolution of the system can be described by the eigenstates  $\psi_p$  of  $H_{\text{eff}}(\mathbf{k})$ . By substituting  $|\psi_i\rangle = \sum_p \langle\psi_p|\psi_i\rangle|\psi_p\rangle$  and  $U(t, t') = \sum_a e^{-i\epsilon_p(t-t')}|\psi_p\rangle\langle\psi_p|$  into equation (C4) and integrating over  $\frac{t+t'}{2}$  and  $t - t'$ , we have:

$$\chi_{zz} = \sum_{pq} 2f_p \frac{\langle\psi_p|s_z|\psi_q\rangle\langle\psi_q|s_z|\psi_p\rangle}{\epsilon_q - \epsilon_p} \quad (\text{D1})$$

with  $f_p = \sum_i f_i |\langle\psi_i|\psi_p\rangle|^2$ .

For the infinite Floquet Hamiltonian  $H_F(\mathbf{k})$  in the Hilbert space of  $\mathcal{H} \otimes \mathcal{L}_T$ , the initial eigenstate  $\psi_i$  is expanded by independent Floquet basis  $\psi_\alpha(t)$  (Floquet states inside the first FBZ):

$$\begin{aligned} \psi_i &= \sum_{\alpha \in \text{FBZ}} \langle\psi_\alpha(t_0)|\psi_i\rangle \psi_\alpha(t_0) \\ &= \sum_{\alpha \in \text{FBZ}} b_{i\alpha} \psi_\alpha(t_0) \\ &= \sum_{\alpha \in \text{FBZ}} b_{i\alpha} e^{-i\epsilon_\alpha t_0} \phi_\alpha(t_0). \end{aligned} \quad (\text{D2})$$

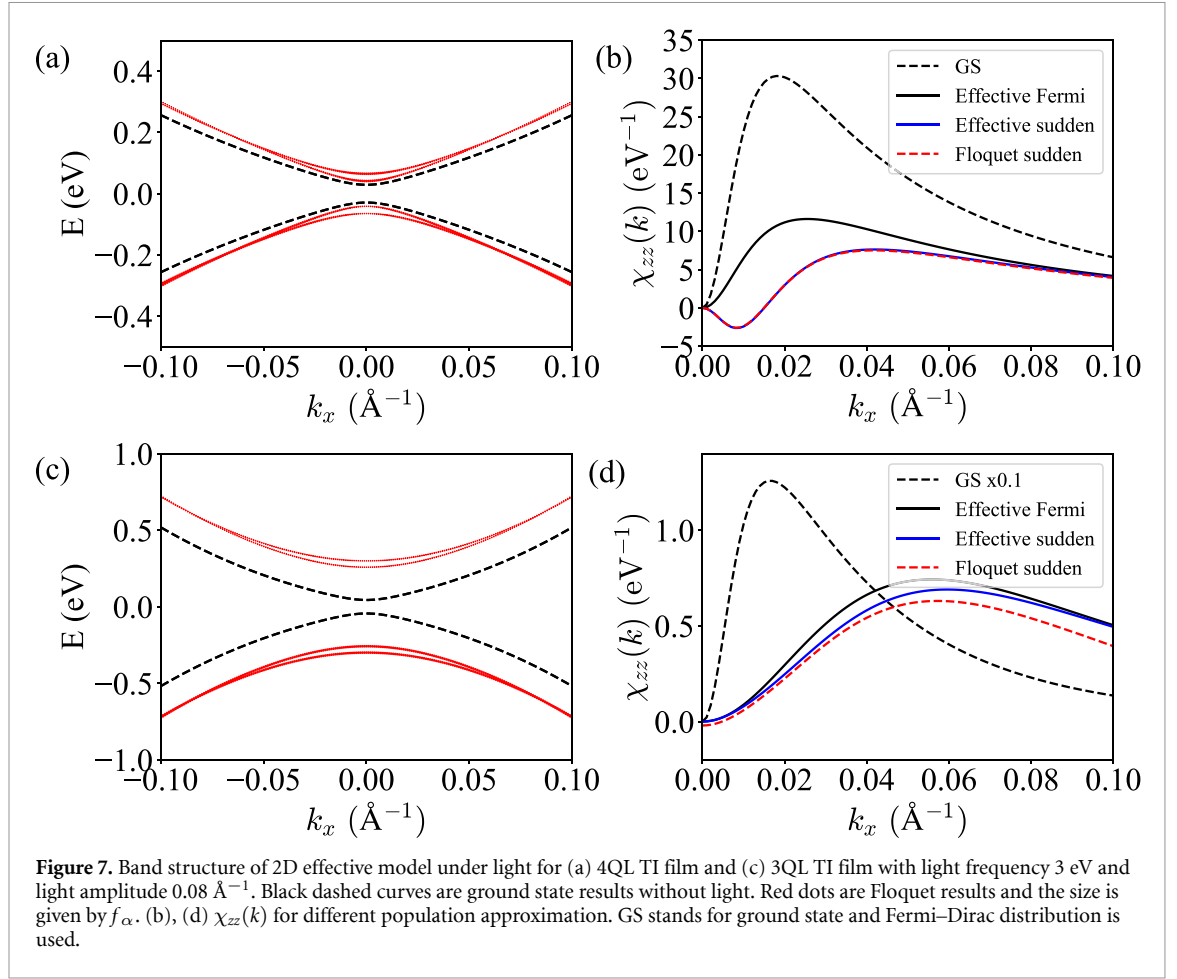
Substitute equations (C3) and (D2) in equation (C4), we get the static spin susceptibility for the Floquet system:

$$\chi_{zz} = \sum_{\alpha \in \text{FBZ}, \beta} 2f_\alpha \frac{|\langle\langle\phi_\alpha(t)|s_z|\phi_\beta(t)\rangle\rangle|^2}{\epsilon_\beta - \epsilon_\alpha}. \quad (\text{D3})$$

Here  $f_\alpha = \sum_i f_i |b_{i\alpha}|^2 = \sum_i f_i |\langle\psi_\alpha(t_0)|\psi_i\rangle|^2$ , acting like the population of Floquet states. Notice that  $\beta$  goes over all possible quasienergies while  $\alpha$  only goes over independent Floquet states. The double bracket is introduced as  $\langle\langle\cdot|\cdot\rangle\rangle = \frac{1}{T} \int_0^T \langle\cdot|\cdot\rangle$  [49].

To show the difference between equations (D1) and (D3), band structures and the  $k$  dependent magnetic susceptibility  $\chi_{zz}(k)$  obtained from  $H_{\text{eff}}(\mathbf{k})$  and  $H_F(\mathbf{k})$  respectively are compared in figure 7. As the amplitude we use here ( $0.08 \text{ \AA}^{-1}$ ) is rather large, the Floquet bands (red solid lines in figures 7(a) and (c)) is quite different from equilibrium (black dashed lines in figures 7(a) and (c)). The susceptibility (figures 7(b) and (d)) is also different in both shape and size compared with equilibrium (black dashed lines in figures 7(b) and (d)). The difference between results obtained from equations (D1) and (D3) (blue and red curves in figure 7(d)) is not very sharp, implying that the system is still in the high-frequency regime.

For clarity, we also calculate the magnetic susceptibility under the Floquet Fermi–Dirac distribution approximation, which is equation (D1) with  $f_a$  replaced by the Fermi–Dirac distribution. The difference between the results from sudden approximation (blue and red curves in figures 7(b) and (d)) and the Floquet Fermi–Dirac approximation (black curve in figures 7(b) and (d)) is significant when band inversion occurs. We observe an obvious population inversion near  $k_x = 0$  for 4QLs (figure 7(b)) rather than 3QLs (figure 7(d)).



## Appendix E. The long-range FM from mean-field theory

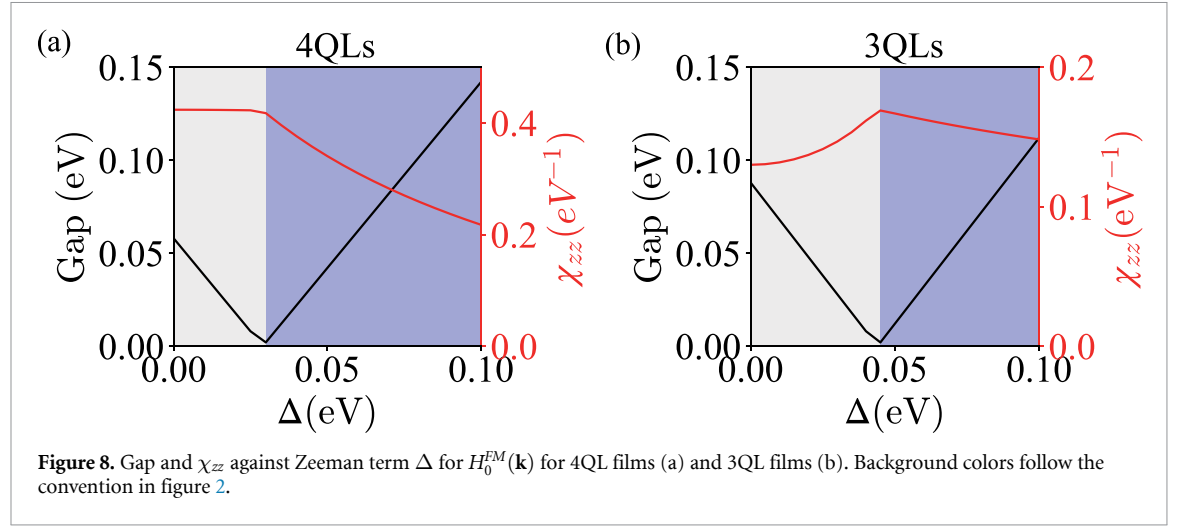
Magnetic properties of this system from the coupling of local moments can be described by  $H_{LM} = -\sum_{ij} \mathcal{J} S_i \cdot S_j$ . Here  $S_i$  represents local moment at site  $i$  and  $\mathcal{J}$  represents effective exchange interactions. To realize robust FM order, we need  $\mathcal{J}$  to be positive.

In our system, two mechanisms [10, 28] mainly contribute to  $\mathcal{J}$ . The first mechanism is the RKKY interaction, namely, a local moment magnetizes nearby band electrons and these band electrons further affect local moments at other sites. This interaction  $\mathcal{J}_F = J^2 \chi$  is FM and proportional to the density of doped magnetic ions and the magnetic susceptibility of band electrons, where  $J$  is the exchange integral between local moment  $S_i$  and band electrons. The second mechanism is the antiferromagnetic superexchange interaction between local moments, which contributes to negative  $\mathcal{J}$  and is proportional to the density of dopant and the inverse Hubbard  $U$  of the local moments  $\mathcal{J} \propto -J^2/U$ . When we fix the dopant density, we need the magnetic susceptibility to satisfy  $\chi > 1/U$  to realize FM order. For typical transition metal ions, it is reasonable to choose  $U = 2.5 \text{ eV}$  [28]. Thus, in our system, the critical spin susceptibility for a possible magnetic PT is around  $0.4 \text{ eV}^{-1}$ . The corresponding critical light amplitudes are indicated in figures 2 and 4 in the main text.

When FM order is developed, the 2D effective Hamiltonian becomes,

$$H_0^{FM}(\mathbf{k}) = H_0(\mathbf{k}) + \Delta \cdot \sigma_3 \otimes I \quad (\text{E1})$$

with an additional Zeeman term  $\Delta$ . As a result, the magnetic susceptibility  $\chi_{zz}$  for  $H_0^{FM}$  now also depends on  $\Delta$ . We plot the gap and  $\chi_{zz}$  against  $\Delta$  in figure 8. The system undergoes a transformation from the trivial phase to the QAH phase at  $\Delta = 0.03 \text{ eV}$  for 4QL films ( $\Delta = 0.045 \text{ eV}$  for 3QLs). During these topological PTs, the spin susceptibility curves also exhibit kinks and then decrease abruptly. We mention that the increase in figure 8(b) is likely due to the band inversion induced by the Zeeman term for 3QL films if the long range FM order is developed. Additionally,  $\Delta$  depends on  $\chi_{zz}$ , necessitating a self-consistent process to solve for both  $\Delta$  and  $\chi_{zz}$  as well as to estimate the Curie temperature.



## Appendix F. Thin film models

Now we fully consider the quantum confinement effects in TI thin films by constructing a film Hamiltonian from a bulk effective  $k \cdot p$  model, which includes contributions from the quantum well states. Following the notion in [68, 74], we start from the effective  $k \cdot p$  model of a Bi<sub>2</sub>Se<sub>3</sub>-type 3D TI at the  $\Gamma$  point in the basis of  $|P1_z^+ \uparrow\rangle, |P2_z^- \uparrow\rangle, |P1_z^+ \downarrow\rangle, |P2_z^- \downarrow\rangle$ :

$$H = \epsilon(k) + \begin{pmatrix} \mathcal{M}(k) & A_1 k_z & 0 & A_2 k_- \\ A_1 k_z & -\mathcal{M}(k) & A_2 k_- & 0 \\ 0 & A_2 k_+ & \mathcal{M}(k) & -A_1 k_z \\ A_2 k_+ & 0 & -A_1 k_z & -\mathcal{M}(k) \end{pmatrix} + O(k^2) \quad (\text{F1})$$

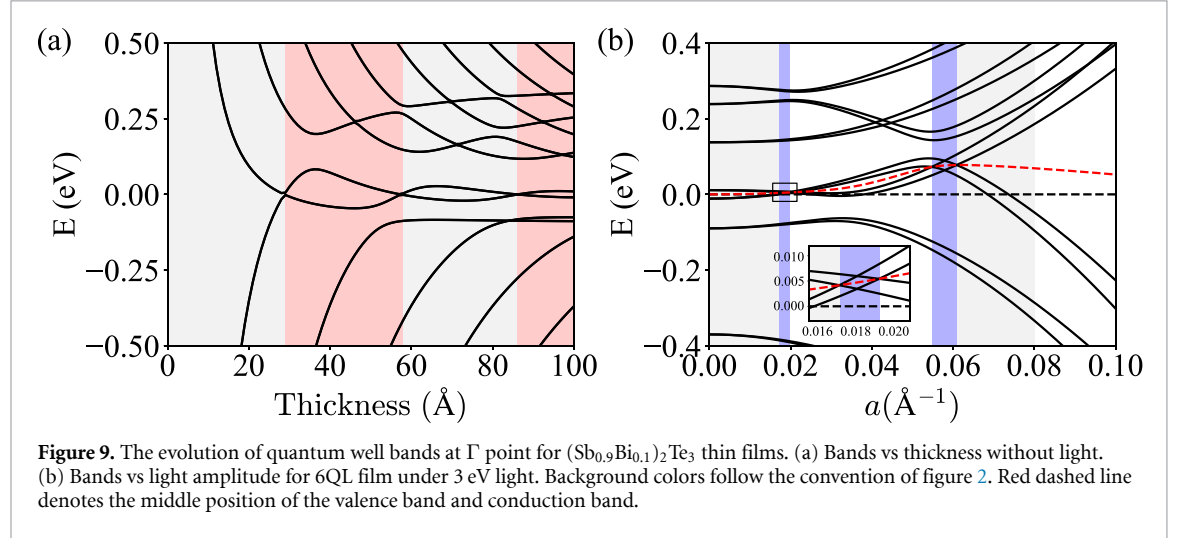
where  $k_{\pm} = k_x \pm i k_y$ ,  $\epsilon(k) = \epsilon_0 + \epsilon_1 k_z^2 + \epsilon_2 (k_x^2 + k_y^2)$  and  $\mathcal{M}(k) = m_0 + m_1 k_z^2 + m_2 (k_x^2 + k_y^2)$ . To construct the Hamiltonian for thin films with fixed boundary condition, we replace  $k_z$  by  $-i\partial_z$  and solve equation (F1) on the quantum well basis [75]  $\psi_n(z) = \sqrt{\frac{2}{d}} \sin(\frac{n\pi z}{d})$ , where  $n = 1, 2, 3, \dots$  and  $d$  is the thickness of the thin film. The following calculations on 6QL ( $d = 60 \text{ \AA}$ ) and 5QL ( $d = 50 \text{ \AA}$ ) (Sb<sub>0.9</sub>Bi<sub>0.1</sub>)<sub>2</sub>Te<sub>3</sub> films are with parameters obtained from [68] by linear interpolation. The parameters are listed in table 1.

According to [75], the topological properties of TI thin films oscillate between a trivial phase and a QSH phase when the thickness increases. This is because more quantum well bands invert as the films become thicker. We plot the band evolution of (Sb<sub>0.9</sub>Bi<sub>0.1</sub>)<sub>2</sub>Te<sub>3</sub> thin films with the change of thickness in figure 9(a).

In this work, we find that the applied laser field also alters the band inversion behavior of the quantum well states. We choose 6QL film as an example. When we increase the light amplitude (see figure 9(b)), these degenerate bands split and invert, inducing four critical laser amplitudes for four gap-closing processes. The splitting of the double-degenerate bands is due to the break of time reversal symmetry by right-handed CPL. The middle position of the gap is denoted by the dashed red line in figure 9(b).

**Table 1.**  $k \cdot p$  parameters for  $(\text{Sb}_{0.9}\text{Bi}_{0.1})_2\text{Te}_3$  films. Unit for  $\epsilon_0$  and  $m_0$  is eV. Unit for  $\epsilon_1$ ,  $\epsilon_2$ ,  $m_1$  and  $m_2$  is  $\text{eV \AA}^2$ . Unit for  $A_1$  and  $A_2$  is  $\text{eV \AA}$ .

$\epsilon_0$	$\epsilon_1$	$\epsilon_2$	$m_0$	$m_1$	$m_2$	$A_1$	$A_2$
-0.0171	-10.496	-4.734	-0.228	17.955	49.397	0.786	3.347



## Appendix G. Problems for sudden approximation

As stated in the main text, the population of Floquet bands under sudden approximation is determined by the overlap between initial and final states when the light is applied. It results in a non-thermal population and could give rise to oscillations of  $\chi_{zz}(k)$  near Floquet band crossings (or avoided-crossings).

There are two types of band crossings in the Floquet systems, one happens between different photon sectors (e.g. the Floquet band with  $m = 0$  crosses with  $m = 1$ ) when the laser frequency is small ( $\hbar\omega < W$ ). And the other happens within one photon sector (e.g. Floquet bands cross each other with same  $m$ ).

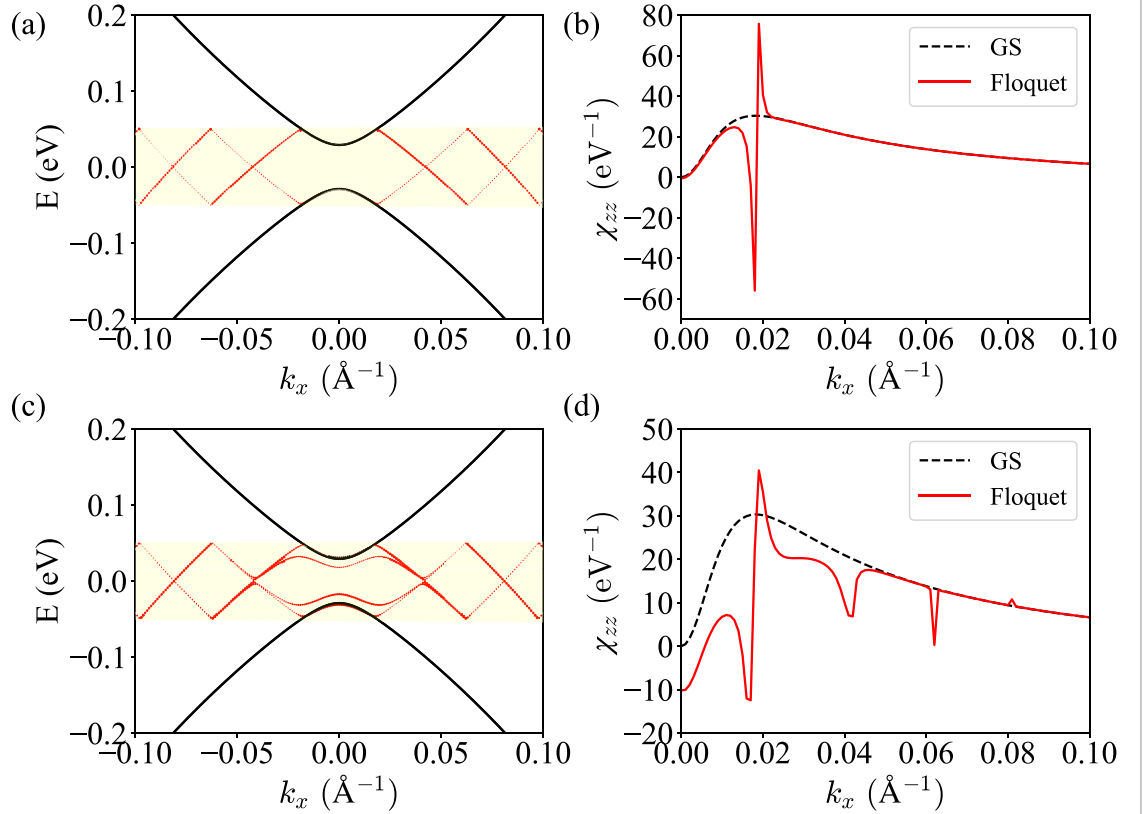
We first discuss the type of crossings between photon sectors with low frequency. Figure 10 presents an example for the 4QL 2D effective model with light driving, where the light frequency ( $\hbar\omega = 0.1$  eV) is chosen to be smaller than the bandwidth to induce band crossings between photon sectors. We consider two laser amplitudes: figures 10(a) and (c) are for amplitude  $0.001 \text{ \AA}^{-1}$  and  $0.01 \text{ \AA}^{-1}$ , respectively. The black curves and red dots represent the band structures from Hamiltonian  $H_0(\mathbf{k})$  without driving light and Floquet Hamiltonian  $H_F(\mathbf{k})$ , respectively. For  $H_F(\mathbf{k})$ , only bands inside FBZ are plotted. Figures 10(b) and (d) show the  $k$  dependent spin susceptibility.

Near band crossing points, as shown in figure 10(b),  $\chi_{zz}(k)$  diverges due to a small energy difference on the denominator of equation (D3) and a nonzero population difference on the numerator. Comparing figures 10(c) with (a), under larger amplitude, we observe contributions from higher Floquet bands and broadening of the divergent peaks. The broadening occurs because the sizes of the avoided-crossing gaps increase with the increase of the light amplitude.

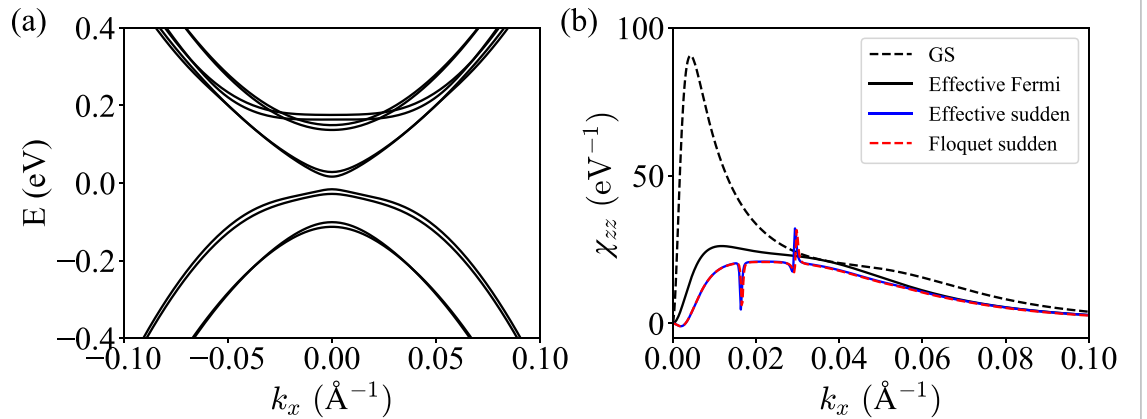
In our framework with sudden approximation, the effect of dissipation is not considered. Based on the Ono and Ishihara's results from the Floquet-Green's function [72], the magnetic susceptibility is continuous with increasing light amplitude. We argue that such kind of divergence is possible to be smeared out by the dissipation.

Figure 11 illustrates the types of crossings that occur inside one photon sector. Here we choose the quantum well model for a 6QL thin film as an example, with a light frequency of 3 eV that is consistent with the main text and larger than the bandwidth to avoid inter-sector crossing. The band structure for  $a = 0.04 \text{ \AA}^{-1}$  is shown in figure 11(a), and  $\chi_{zz}(k)$  is displayed in figure 11(b). We observe divergent peaks in susceptibility when bands cross with each other.





**Figure 10.** Band structures of 2D effective model for 4QL film under light frequency 0.1 eV and light amplitude (a) 0.001 Å<sup>-1</sup> and (c) 0.01 Å<sup>-1</sup>. Black curves and red dots are results from Hamiltonian without driving light and infinite Floquet Hamiltonian respectively. The size of the red dots is given by  $f_{\alpha}$ . The yellow background stands for the first FBZ. (b) and (d)  $k$  dependent  $\chi_{zz}(k)$  for  $H_0(\mathbf{k})$  under Fermi–Dirac distribution (black dashed line) and  $H_F(\mathbf{k})$  under sudden approximation respectively.



**Figure 11.** (a) Band structure of quantum well model for 6QL thin film under the light ( $\hbar\omega = 3$  eV). The amplitude is 0.04 Å<sup>-1</sup>. (b)  $\chi_{zz}(k)$  for ground state with Fermi–Dirac distribution and Floquet Hamiltonian  $H_F(\mathbf{k})$  with sudden approximation.

## Appendix H. Light intensity

In our work, we adopt effective light amplitude  $a$  for simplicity as it is in unit of Å<sup>-1</sup>. In this section, we discuss the relation between light intensity and the effective light amplitude  $a$ . The relation between light intensity and light electric field is  $I = \frac{1}{2}cn\epsilon_0 E^2$ , in which  $\epsilon_0$  is the vacuum permittivity,  $c$  is the speed of light, and  $n$  is the refractive index of the TI thin film [76]. In the experiment, the light intensity can be achieved as high as 10<sup>12</sup> W cm<sup>-2</sup>, which corresponds to 0.2/ $\hbar\omega$  for effective light amplitude  $a$ . Thus our proposed critical amplitudes are possible to be achieved in experiments.

## ORCID iDs

Benshu Fan  <https://orcid.org/0000-0003-3845-5855>

Hannes Hübener  <https://orcid.org/0000-0003-0105-1427>

Umberto De Giovannini  <https://orcid.org/0000-0002-4899-1304>

Wenhui Duan  <https://orcid.org/0000-0001-9685-2547>

Angel Rubio  <https://orcid.org/0000-0003-2060-3151>

Peizhe Tang  <https://orcid.org/0000-0002-6345-5809>

## References

- [1] Armitage N P, Mele E J and Vishwanath A 2018 Weyl and dirac semimetals in three dimensional solids *Rev. Mod. Phys.* **90** 015001
- [2] Xu G, Weng H M, Wang Z J, Dai X and Fang Z 2011 Chern semimetal and the quantized anomalous Hall effect in  $\text{HgCr}_2\text{Se}_4$  *Phys. Rev. Lett.* **107** 186806
- [3] Yang H, Sun Y, Zhang Y, Shi W-J, Parkin S S P and Yan B 2017 Topological Weyl semimetals in the chiral antiferromagnetic materials  $\text{Mn}_3\text{Ge}$  and  $\text{Mn}_3\text{Sn}$  *New J. Phys.* **19** 015008
- [4] Liu E et al 2018 Giant anomalous Hall effect in a ferromagnetic kagome-lattice semimetal *Nat. Phys.* **14** 1125–31
- [5] Qin P et al 2022 Chemical potential switching of the anomalous Hall effect in an ultrathin noncollinear antiferromagnetic metal *Adv. Mater.* **34** 2200487
- [6] Kuroda K et al 2017 Evidence for magnetic Weyl fermions in a correlated metal *Nat. Mater.* **16** 1090–5
- [7] Chang G et al 2017 Topological hopf and chain link semimetal states and their application to  $\text{Co}_2\text{MnGa}$  *Phys. Rev. Lett.* **119** 156401
- [8] Tang P, Zhou Q, Xu G and Zhang S-C 2016 Dirac fermions in an antiferromagnetic semimetal *Nat. Phys.* **12** 1100–4
- [9] Wang J 2017 Antiferromagnetic Dirac semimetals in two dimensions *Phys. Rev. B* **95** 115138
- [10] Yu R, Zhang W, Zhang H-J, Zhang S-C, Dai X and Fang Z 2010 Quantized anomalous Hall effect in magnetic topological insulators *Science* **329** 61–64
- [11] Chang C-Z et al 2013 Experimental observation of the quantum anomalous Hall effect in a magnetic topological insulator *Science* **340** 167–70
- [12] Kou X et al 2014 Scale-invariant quantum anomalous Hall effect in magnetic topological insulators beyond the two-dimensional limit *Phys. Rev. Lett.* **113** 137201
- [13] Checkelsky J, Yoshimi R, Tsukazaki A, Takahashi K S, Kozuka Y, Falson J, Kawasaki M and Tokura Y 2014 Trajectory of the anomalous Hall effect towards the quantized state in a ferromagnetic topological insulator *Nat. Phys.* **10** 731–6
- [14] Feng Y et al 2015 Observation of the zero Hall plateau in a quantum anomalous Hall insulator *Phys. Rev. Lett.* **115** 126801
- [15] Chang C-Z et al 2015 High-precision realization of robust quantum anomalous Hall state in a hard ferromagnetic topological insulator *Nat. Mater.* **14** 473–7
- [16] Xu G, Lian B and Zhang S-C 2015 Intrinsic quantum anomalous Hall effect in the kagome lattice  $\text{Cs}_2\text{LiMn}_3\text{F}_{12}$  *Phys. Rev. Lett.* **115** 186802
- [17] Mong R S K, Essin A M and Moore J E 2010 Antiferromagnetic topological insulators *Phys. Rev. B* **81** 245209
- [18] Li J, Li Y, Du S, Wang Z, Gu B-L, Zhang S-C, He K, Duan W and Xu Y 2019 Intrinsic magnetic topological insulators in van der Waals layered  $\text{MnBi}_2\text{Te}_4$ -family materials *Sci. Adv.* **5** eaaw5685
- [19] Li R, Wang J, Qi X-L and Zhang S-C 2010 Dynamical axion field in topological magnetic insulators *Nat. Phys.* **6** 284–8
- [20] Wan X, Vishwanath A and Savrasov S Y 2012 Computational design of axion insulators based on 5 *d* spinel compounds *Phys. Rev. Lett.* **108** 146601
- [21] Mogi M, Kawamura M, Yoshimi R, Tsukazaki A, Kozuka Y, Shirakawa N, Takahashi K, Kawasaki M and Tokura Y 2017 A magnetic heterostructure of topological insulators as a candidate for an axion insulator *Nat. Mater.* **16** 516–21
- [22] Xiao D et al 2018 Realization of the axion insulator state in quantum anomalous Hall sandwich heterostructures *Phys. Rev. Lett.* **120** 056801
- [23] Zhang D, Shi M, Zhu T, Xing D, Zhang H and Wang J 2019 Topological axion states in the magnetic insulator  $\text{MnBi}_2\text{Te}_4$  with the quantized magnetoelectric effect *Phys. Rev. Lett.* **122** 206401
- [24] Liu Q, Liu C-X, Xu C, Qi X-L and Zhang S-C 2009 Magnetic impurities on the surface of a topological insulator *Phys. Rev. Lett.* **102** 156603
- [25] Checkelsky J G, Ye J, Onose Y, Iwasa Y and Tokura Y 2012 Dirac-fermion-mediated ferromagnetism in a topological insulator *Nat. Phys.* **8** 729–33
- [26] Chang C-Z et al 2013 Thin films of magnetically doped topological insulator with carrier-independent long-range ferromagnetic order *Adv. Mater.* **25** 1065
- [27] Zhang J et al 2013 Topology-driven magnetic quantum phase transition in topological insulators *Science* **339** 1582–6
- [28] Wang J, Lian B and Zhang S-C 2015 Electrically tunable magnetism in magnetic topological insulators *Phys. Rev. Lett.* **115** 036805
- [29] Zhang Z et al 2017 Magnetic quantum phase transition in Cr-doped  $\text{Bi}_2(\text{Se}_x\text{Te}_{1-x})_3$  driven by the stark effect *Nat. Nano* **12** 953–7
- [30] Oka T and Kitamura S 2018 Floquet engineering of quantum materials *Annu. Rev. Condens. Matter Phys.* **10** 387–408
- [31] Hübener H, Sentef M A, De Giovannini U, Kemper A F and Rubio A 2017 Creating stable Floquet–Weyl semimetals by laser-driving of 3D Dirac materials *Nat. Commun.* **8** 13940
- [32] Hübener H, De Giovannini U and Rubio A 2018 Phonon driven Floquet matter *Nano Lett.* **18** 1535–42
- [33] Shin D, Hübener H, De Giovannini U, Jin H, Rubio A and Park N 2018 Phonon-driven spin-Floquet magneto-valleytronics in  $\text{MoS}_2$  *Nat. Commun.* **9** 638
- [34] Shin D, Sato S A, Hübener H, De Giovannini U, Kim J, Park N and Rubio A 2019 Unraveling materials Berry curvature and Chern numbers from real-time evolution of Bloch states *Proc. Natl Acad. Sci.* **116** 4135–40
- [35] Bao C, Tang P, Sun D and Zhou S 2022 Light-induced emergent phenomena in 2D materials and topological materials *Nat. Rev. Phys.* **4** 33–48
- [36] Kirilyuk A, Kimel A V and Rasing T 2010 Ultrafast optical manipulation of magnetic order *Rev. Mod. Phys.* **82** 2731
- [37] Buzzi M, Först M, Mankowsky R and Cavalleri A 2018 Probing dynamics in quantum materials with femtosecond x-rays *Nat. Rev. Mater.* **3** 299–311

- [38] Kitagawa T, Berg E, Rudner M and Demler E 2010 Topological characterization of periodically driven quantum systems *Phys. Rev. B* **82** 235114
- [39] Wang Y H, Steinberg H, Jarillo-Herrero P and Gedik N 2013 Observation of Floquet–Bloch states on the surface of a topological insulator *Science* **342** 453–7
- [40] Mahmood F, Chan C-K, Alpichshev Z, Gardner D, Lee Y, Lee P A and Gedik N 2016 Selective scattering between Floquet–Bloch and Volkov states in a topological insulator *Nat. Phys.* **12** 306–10
- [41] Wang Z F, Liu Z, Yang J and Liu F 2018 Light-induced type-ii band inversion and quantum anomalous Hall state in monolayer FeSe *Phys. Rev. Lett.* **120** 156406
- [42] Liu H, Sun J-T, Cheng C, Liu F and Meng S 2018 Photoinduced nonequilibrium topological states in strained black phosphorus *Phys. Rev. Lett.* **120** 237403
- [43] Zhou S et al 2023 Pseudospin-selective Floquet band engineering in black phosphorus *Nature* **614** 75–80
- [44] Liu W, Ke Y, Zhu B and Lee C 2020 Modulation-induced long-range magnon bound states in one-dimensional optical lattices *New J. Phys.* **22** 093052
- [45] Lindner N H, Refael G and Galitski V 2011 Floquet topological insulator in semiconductor quantum wells *Nat. Phys.* **7** 490–5
- [46] D’lessio L and Rigol M 2015 Dynamical preparation of Floquet Chern insulators *Nat. Commun.* **6** 8336
- [47] Seetharam K I, Bardyn C E, Lindner N H, Rudner M S and Refael G 2015 Controlled population of Floquet-Bloch states via coupling to bose and fermi baths *Phys. Rev. X* **5** 041050
- [48] Claassen M, Jia C, Moritz B and Devereaux T P 2016 All-optical materials design of chiral edge modes in transition-metal dichalcogenides *Nat. Commun.* **7** 13074
- [49] Oka T and Aoki H 2009 Photovoltaic Hall effect in graphene *Phys. Rev. B* **79** 081406
- [50] Dehghani H, Oka T and Mitra A 2014 Dissipative Floquet topological systems *Phys. Rev. B* **90** 195429
- [51] Dehghani H, Oka T and Mitra A 2015 Out-of-equilibrium electrons and the Hall conductance of a Floquet topological insulator *Phys. Rev. B* **91** 155422
- [52] Zhai X and Jin G 2014 Photoinduced topological phase transition in epitaxial graphene *Phys. Rev. B* **89** 235416
- [53] Perez-Piskunow P M, Usaj G, Balseiro C A and Torres L E F F 2014 Floquet chiral edge states in graphene *Phys. Rev. B* **89** 121401
- [54] Sentef M A, Claassen M, Kemper A F, Moritz B, Oka T, Freericks J K and Devereaux T P 2015 Theory of Floquet band formation and local pseudospin textures in pump-probe photoemission of graphene *Nat. Commun.* **6** 7047
- [55] McIver J W, Schulte B, Stein F-U, Matsuyama T, Jotzu G, Meier G and Cavalleri A 2020 Light-induced anomalous Hall effect in graphene *Nat. Phys.* **16** 38–41
- [56] Sato S A et al 2019 Microscopic theory for the light-induced anomalous Hall effect in graphene *Phys. Rev. B* **99** 214302
- [57] Shirley J H 1965 Solution of the Schrödinger equation with a Hamiltonian periodic in time *Phys. Rev. B* **138** 979–87
- [58] Sambe H 1973 Steady states and quasienergies of a quantum-mechanical system in an oscillating field *Phys. Rev. A* **7** 2203–13
- [59] Grifoni M and Hänggi P 1998 Driven quantum tunneling *Phys. Rep.* **304** 229–354
- [60] Eckardt A and Anisimovas E 2015 High-frequency approximation for periodically driven quantum systems from a Floquet-space perspective *New J. Phys.* **17** 093039
- [61] See supplemental material, which includes [76], for the details on the Floquet Theory, charge populations, Kubo formula, thin film model and light intensity
- [62] Kirilyuk A, Kimel A V and Rasing T 2010 Ultrafast optical manipulation of magnetic order *Rev. Mod. Phys.* **82** 2731
- [63] Iadecola T, Neupert T and Chamon C 2015 Occupation of topological Floquet bands in open systems *Phys. Rev. B* **91** 235133
- [64] Stefanucci G and van Leeuwen R 2013 *Nonequilibrium Many-Body Theory of Quantum Systems: A Modern Introduction* (Cambridge: Cambridge University Press)
- [65] Chen Q, Du L and Fiete G A 2018 Floquet band structure of a semi-dirac system *Phys. Rev. B* **97** 035422
- [66] Zhang Y et al 2010 Crossover of the three-dimensional topological insulator Bi<sub>2</sub>Se<sub>3</sub> to the two-dimensional limit *Nat. Phys.* **6** 584–8
- [67] Shan W-Y, Lu H-Z and Shen S-Q 2010 Effective continuous model for surface states and thin films of three-dimensional topological insulators *New J. Phys.* **12** 043048
- [68] Liu C-X, Qi X-L, Zhang H, Dai X, Fang Z and Zhang S-C 2010 Model Hamiltonian for topological insulators *Phys. Rev. B* **82** 045122
- [69] Mikami T, Kitamura S, Yasuda K, Tsuji N, Oka T and Aoki H 2015 Brillouin-Wigner theory for high-frequency expansion in periodically driven systems: application to Floquet topological insulators *Phys. Rev. B* **93** 144307
- [70] Sie E J, Lui C H, Lee Y-H, Fu L, Kong J and Gedik N 2017 Large, valley-exclusive Bloch–Siegert shift in monolayer WS<sub>2</sub> *Science* **355** 1066–9
- [71] Aeschlimann S et al 2021 Survival of Floquet–Bloch states in the presence of scattering *Nano Lett.* **21** 5028–35
- [72] Ono A and Ishihara S 2019 Nonequilibrium susceptibility in photoinduced Floquet states *Phys. Rev. B* **100** 075127
- [73] Xu H, Zhou J, Wang H and Li J 2021 Light-induced static magnetization: nonlinear edelstein effect *Phys. Rev. B* **103** 205417
- [74] Zhang H, Liu C-X, Qi X-L, Dai X, Fang Z and Zhang S-C 2009 Topological insulators in Bi<sub>2</sub>Se<sub>3</sub>, Bi<sub>2</sub>Te<sub>3</sub> and Sb<sub>2</sub>Te<sub>3</sub> with a single Dirac cone on the surface *Nat. Phys.* **5** 438–42
- [75] Liu C-X, Zhang H J, Yan B, Qi X-L, Frauenheim T, Dai X, Fang Z and Zhang S-C 2010 Oscillatory crossover from two-dimensional to three-dimensional topological insulators *Phys. Rev. B* **81** 041307
- [76] Yue Z, Chen Q, Sahu A, Wang X and Gu M 2017 Photo-oxidation-modulated refractive index in Bi<sub>2</sub>Te<sub>3</sub> thin films *Mater. Res. Express* **4** 126403